ISSN 1674-1056
http://cpb.iphy.ac.cn
http://iopscience.iop.org/cpb
中国物理 B
Chinese Physics
中国物理 Chinese Physics B

Phase diagram, correlations, and quantum critical point in the periodic Anderson model

Jian-Wei Yang(杨建伟), Qiao-Ni Chen(陈巧妮)
Citation: Chin. Phys. B . 2018, 27(3): 037101. **doi:** 10.1088/1674-1056/27/3/037101

Journal homepage: http://cpb.iphy.ac.cn; http://iopscience.iop.org/cpb

What follows is a list of articles you may be interested in

Effect of anionic ordering on the electronic and optical properties of $BaTaO_2N$: TB-mBJ density functional calculation

K Bettine, O Sahnoun, M Sahnoun, M Driz
Chin. Phys. B . 2017, 26(5): 057101. **doi:** 10.1088/1674-1056/26/5/057101

Electrical property effect of oxygen vacancies in the heterojunction of $LaGaO_3/SrTiO_3$

Fu-Ning Wang(王芙凝), Ji-Chao Li(李吉超), Xin-Miao Zhang(张鑫淼), Han-Zhang Liu(刘汉璋), Jian Liu(刘剑), Chun-Lei Wang(王春雷), Ming-Lei Zhao(赵明磊), Wen-Bin Su(苏文斌), Liang-Mo Mei(梅良模)
Chin. Phys. B . 2017, 26(3): 037101. **doi:** 10.1088/1674-1056/26/3/037101

Structural, electronic, and magnetic properties of vanadium atom-adsorbed $MoSe_2$ monolayer

Ping Liu(刘萍), Zhen-Zhen Qin(秦真真), Yun-Liang Yue(乐云亮), Xu Zuo(左旭)
Chin. Phys. B . 2017, 26(2): 027103. **doi:** 10.1088/1674-1056/26/2/027103

Band offsets engineering at $Cd_xZn_{1-x}S/Cu_2ZnSnS_4$ heterointerface

Wujisiguleng Bao(包乌吉斯古楞), Sachuronggui(萨初荣贵), Fang-Yuan Qiu(仇方圆)
Chin. Phys. B . 2016, 25(12): 127102. **doi:** 10.1088/1674-1056/25/12/127102

First-principles studies of effects of interstitial boron and carbon on the structural, elastic, and electronic properties of Ni solution and Ni_3Al intermetallics

Meng-Li Huang(黄梦礼), Chong-Yu Wang(王崇愚)
Chin. Phys. B . 2016, 25(10): 107104. **doi:** 10.1088/1674-1056/25/10/107104

Phase diagram, correlations, and quantum critical point in the periodic Anderson model*

Jian-Wei Yang(杨建伟) and Qiao-Ni Chen(陈巧妮)†

Department of Physics, Beijing Normal University, Beijing 100875, *China*

(Received 10 November 2017; revised manuscript received 1 December 2017; published online 11 February 2018)

Periodic Anderson model is one of the most important models in the field of strongly correlated electrons. With the recent developed numerical method density matrix embedding theory, we study the ground state properties of the periodic Anderson model on a two-dimensional square lattice. We systematically investigate the phase diagram away from half filling. We find three different phases in this region, which are distinguished by the local moment and the spin–spin correlation functions. The phase transition between the two antiferromagnetic phases is of first order. It is the so-called Lifshitz transition accompanied by a reconstruction of the Fermi surface. As the filling is close to half filling, there is no difference between the two antiferromagnetic phases. From the results of the spin–spin correlation, we find that the Kondo singlet is formed even in the antiferromagnetic phase.

Keywords: periodic Anderson model, Kondo singlet states, density matrix embedding theory

PACS: 71.10.–w, 71.10.Fd, 71.10.Hf, 75.20.Hr **DOI:** 10.1088/1674-1056/27/3/037101

1. Introduction

Heavy fermion materials[1] display abnormal behaviors in many respects, such as large magnetic susceptibility and specific-heat coefficient,[2] unconventional superconductivity,[3–6] and non-Fermi liquid behavior.[7] Most of the heavy fermion compounds contain rare earth elements with partially filled f shells. The unusual properties of the heavy fermion compounds are usually attributed to the admixture of the local f orbital with the conduction band. Kondo lattice model (KLM) and periodic Anderson model (PAM)[8] are believed to capture the physics of the heavy fermion materials. KLM can be derived from PAM by fixing the filling of the f orbital to 1 at the large U limit. PAM is an asymmetric two-band model, which contains conduction c orbital and correlated f orbital. Although simple, it displays rich physics, such as the valence fluctuation,[9] the appearance of Lifshitz transition,[10–12] and the competition between the Ruderman–Kittel–Kasuya–Yosida (RKKY) interaction and the Kondo interaction.[13–15]

Among the above phenomena, the Lifshitz transition is of particular interest. A transition associated with the change of Fermi surface topology is the so-called Lifshitz transition.[16] There have been several experiments exhibiting the Lifshitz transition in heavy fermion materials. The Hall coefficient of $YbRh_2Si_2$ shows a rapid change as a function of the magnetic field,[17] and this can be interpreted by the collapse of the large Fermi surface. Measurement of De Haas–van Alphen effect on $CeRh_{1-x}Co_xIn_5$ shows a Fermi surface reconstruction as a function of x.[18] A Fermi surface reconstruction is also observed in the antiferromagnetic phase of $CeRhI_5$ under a magnetic field.[19] Recent angle-resolved photoemission spectroscopy measurement on $YbAl_3$ discovers that the Lifshitz transition could be caused by the valence fluctuation.[20]

Meanwhile there are many theoretical studies about the Lifshitz transitions on models, including studies on Kondo lattice model[21–23] and periodic Anderson model.[10–12] The mean field theory is widely used in the above studies. It could be applied to any parameters, but it is not a many-body method. By introducing Gutzwiller projection, variational Monte Carlo simulation has many-body nature, but it quite relies on the trial wavefunctions. Dynamical mean field theory (DMFT) avoids these problems, but it makes a simplified treatment of the interactions. In this work, we use the density matrix embedding theory (DMET) to study the ground state properties of the two-dimensional PAM. DMET is a quantum cluster method the same as DMFT, but it does not have bath discretization error and can be practically computed without analytic continuation.

This paper is organized as follows. In Section 2, we briefly describe the model and provide details of the method. Our main results on the phase diagrams, physical quantities and discussion are included in Section 3. Finally, a summary is provided in Section 4.

2. Model and method

We study the periodic Anderson model on a two-dimensional square lattice. The Hamiltonian reads

$$H = -t\sum_{\langle ij\rangle\sigma}(c^{\dagger}_{i\sigma}c_{j\sigma}+\text{h.c.})+E_f\sum_{i\sigma}f^{\dagger}_{i\sigma}f_{i\sigma}$$

*Project supported by the National Natural Science Foundation of China (Grant No. 11504023).

†Corresponding author. E-mail: qiaoni@bnu.edu.cn

© 2018 Chinese Physical Society and IOP Publishing Ltd

$$+V\sum_{i\sigma}(c^{\dagger}_{i\sigma}f_{i\sigma}+\text{h.c.})+U\sum_{i}n^{f}_{i\uparrow}n^{f}_{i\downarrow}, \tag{1}$$

where $c^{\dagger}_{i\sigma}$ ($c_{i\sigma}$) and $f^{\dagger}_{i\sigma}$ ($f_{i\sigma}$) are the creation (annihilation) operators for the conduction and localized orbitals on site i with spin σ, respectively, t is the hopping integral between the neighboring conduction orbitals, E_f is the on-site energy of the localized orbital (f state), which defines the relative position of the f state with respect to the Fermi energy of the conduction orbital (c state), V is the hybridization strength between the c and f states on the same site, and U is the on-site Coulomb repulsion of the f states. $n^{f}_{i\sigma}$ is the number of f electrons on site i with spin σ.

Density matrix embedding theory was first proposed in 2012,[24] since then it has been applied to several different systems, including the Hubbard model,[25–28] the interacting electron–phonon model,[29] and the *ab-initio* quantum chemistry problem.[30–32] By introducing an auxiliary noninteracting system, DMET maps the original lattice model to an interacting quantum impurity model, then solves the impurity model exactly. The impurity model and the auxiliary system are linked by a self-consistency condition of the one-particle-reduced-density-matrix (1-PDM). By construction, the number of bath orbitals in DMET is finite, thus there is no bath discretization error and the computational cost is much lower.

Like the other quantum cluster methods, DMET first divides the lattice sites into different clusters, which tile the whole lattice. In order to keep the translational invariance, we always choose clusters to be unit cells of the lattice. Then the auxiliary Hamiltonian h is

$$h = h_0 + v, \tag{2}$$

where h_0 is the one body term of H, and v is the correlation potential within the cluster. In this work, we do not consider the superconducting phase, so v has the form

$$v = \sum_{C}\sum_{i,j\in C} v_{ij\sigma}c^{\dagger}_{i\sigma}c_{j\sigma}. \tag{3}$$

Here C is the cluster that we partition the lattice into. Since the correlation potential is only within the cluster, it is block diagonal. It can be considered as an approximation of the local interaction.

From the ground state $|\Phi\rangle$ of h, the embedding basis could be constructed. We choose the sites in one of the clusters as the impurity sites, and the sites from the rest of the clusters as the environment sites. There are several mathematically equivalent unitary transformations (we do not get into the details here, for more details, please read Ref. [27]). By applying the transformation, all the orbitals from the environment sites linearly combine into bath orbitals, core orbitals, and virtual orbitals. The core (virtual) orbitals are completely empty (full), thus only the bath orbitals are entangled with the impurity orbitals. By applying the projection operator P which projects the Hamiltonian h into the space spanned by the impurity orbitals and bath orbitals, removing the correlation potential on the impurity orbitals, and bringing back interactions on the impurity orbitals, we can obtain the impurity Hamiltonian H_{imp}

$$H_{\text{imp}} = PhP - \sum_{i,j\in\text{imp}} v_{ij}c^{\dagger}_{i\sigma}c_{j\sigma} + U\sum_{i\in\text{imp}} n^{f}_{i\uparrow}n^{f}_{i\downarrow}. \tag{4}$$

Only the bath orbitals and impurity orbitals constitute the impurity model H_{imp}. Because the bath orbitals are at most as many as the impurity orbitals, the impurity model can be solved exactly. In this work, we use the density matrix renormalization group (DMRG) method[33] to solve the impurity model H_{imp}.

As we mentioned previously, with the 1-PDM ρ^{I} of H_{imp}, the correlation potential is determined by a self-consistent procedure. Our goal is to minimize the difference of ρ^{I} and 1-PDM ρ^{0} which is derived by downfolding $|\Phi\rangle$ to the impurity and bath space

$$\min_{v} f(v) = \sqrt{\sum_{ij}|\rho^{\text{I}}_{ij} - \rho^{0}_{ij}|^2}. \tag{5}$$

When optimizing $f(v)$, the ground state of H_{imp} is fixed, the optimal v is used to update $|\Phi\rangle$, so does ρ^{0}. Then the impurity Hamiltonian H_{imp} as well as ρ^{I} are updated too. Thus the self-consistent loop is formed.

In summary, the DMET calculation include the following steps. (i) Choose an initial guess of the correlation potential v_0. (ii) Solve the auxiliary lattice Hamiltonian to obtain the lattice wave function $|\Phi\rangle$. (iii) The embedding basis is constructed from the lattice wave function $|\Phi\rangle$. (iv) Transform to the embedding basis, and add the interaction to obtain the impurity model. (v) Use the DMRG impurity solver to compute the ground state of the impurity model, and calculate the corresponding one particle reduced density matrix. (vi) Update the correlation potential v to minimize the difference of the one particle reduced density matrix between the auxiliary Hamiltonian h and the impurity Hamiltonian H_{imp}. (vii) Go back to step (ii) until the correlation potential v converges.

3. Results

We have run the DMET calculation of PAM on a two-dimensional square lattice. The lattice size of our calculation is 72×72, and the cluster we used is 1×2 or 2×2. From Figs. 2 and 3, we can see that the calculations with the 1×2 and 2×2 clusters produce almost the same results. There is not so much finite cluster error in this work. The following results are all done by fixing the on-site Coulomb repulsion U to 8.0 (hopping integral $t=1$), since there have been many discussions on the U–V phase diagram.

We show the ground state V–E_f phase diagrams in Fig. 1. As E_f increases, there are three different phases: antiferromagnetic phase 2 (AF2), antiferromagnetic phase 1 (AF1), and paramagnetic Kondo singlet phase (PKS). The local moment is nonzero in both AF1 and AF2 phases, while it is zero in the PKS phase. There is a Fermi surface reconstruction between the AF1 and AF2 phases, which leads to a first-order phase transition between the two antiferromagnetic phases. At filling $n = 1.75$, the AF1 phase only appears at small value of V, while at filling $n = 1.917$, the AF2 phase shrinks, and the AF1 phase amplifies. When E_f is fixed to -1 at filling $n = 1.75$, one could go through the AF2 phase directly to the PKS phase. At filling $n = 1.917$, if one fixes $E_f = -1$, the AF1 phase is between the AF2 phase and PKS phase.

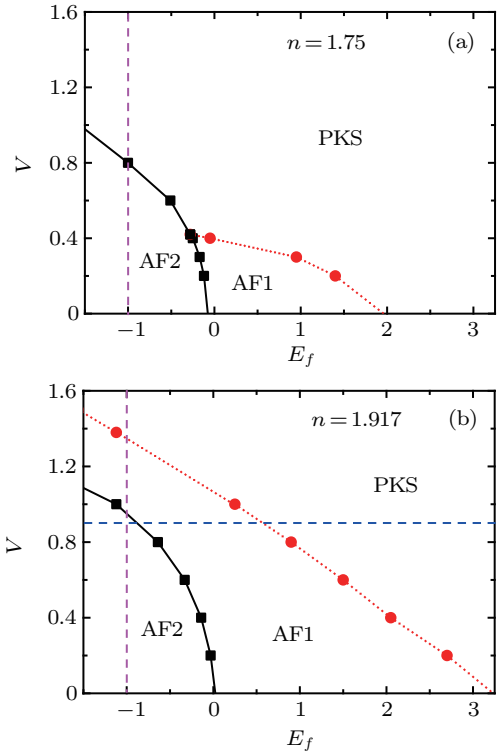


Fig. 1. (color online) The V–E_f phase diagrams at different fillings: (a) $n = 1.75$ and (b) $n = 1.917$. There are three different phases. AF2 and AF1 are two antiferromagnetic phases with different forms of Fermi surface, and PKS stands for the paramagnetic Kondo singlet phase. The black line is the phase boundary between the AF2 and AF1 phases, while the red dotted line is the phase boundary between the AF1 phase and PKS phase.

Now we discuss how the physical quantities change in different phases. The number of electrons and the local moment are defined as

$$\begin{aligned} n_i^\alpha &= \langle n_{i\uparrow}^\alpha + n_{i\downarrow}^\alpha \rangle, \\ m_i^\alpha &= \langle n_{i\uparrow}^\alpha - n_{i\downarrow}^\alpha \rangle. \end{aligned} \tag{6}$$

Here $n_{i\sigma}^\alpha$ is the number of spin σ electrons of α orbital on site i. First we go through the horizontal dashed line (blue line) in Fig. 1(b) by fixing the hybridization V to 0.9 at filling $n = 1.917$. The results are displayed in Fig. 2. The local magnetic moment and the number of electrons are shown in Figs. 2(a) and 2(c). $E_f = -U/2$ is the symmetric case where the Fermi energy of the conduction orbitals is in the middle of the two f orbital energy levels. The number of f states (n_f) and c states (n_c) are both 1.0 at the half filling symmetric case. Away from half filling, n_f is close to 1.0, while n_c is slightly smaller than 1.0. As E_f increases, the electrons are more and more likely to occupy the c states, so n_c increases while n_f decreases. The value of V is small here, so the RKKY effect dominates, there is an antiferromagnet long range order in both the f orbitals and the c orbitals. The localized f orbitals have larger local moments, while the conduction c orbitals have smaller local moments. There is antiferromagnetic coupling between the f and c orbitals on the same site, thus m_f and m_c always have the opposite signs. The local moments decrease as E_f increases and become zero in the paramagnetic phase. Before the magnetic transition occurs, both local moment and number of electrons have a discontinuity. It is due to the Fermi surface reconstruction which causes a first order phase transition. This is the so-called Lifshitz transition.

In order to understand the magnetic properties, we also calculate the spin–spin correlation functions. The correlation functions are defined as

$$\begin{aligned} C_{ff}(r=1) &= \langle (n_{i\uparrow}^f - n_{i\downarrow}^f)(n_{j\uparrow}^f - n_{j\downarrow}^f) \rangle = \langle m_i^f \cdot m_j^f \rangle, \\ C_{fd}(r=0) &= \langle (n_{i\uparrow}^f - n_{i\downarrow}^f)(n_{i\uparrow}^c - n_{i\downarrow}^c) \rangle = \langle m_i^f \cdot m_i^c \rangle. \end{aligned} \tag{7}$$

The results of the spin–spin correlation functions are shown in Figs. 2(b) and 2(d). Figure 2(b) is the correlation function between neighboring f states $C_{ff}(r = 1)$. In the AF2 and AF1 phases, it has a non-zero value. There is a discontinuity at the transition point between the two phases as another evidence of the Lifshitz transition. As the antiferromagnetic long range order disappears in the PKS phase, $C_{ff}(r = 1)$ soon becomes zero.

Figure 2(d) is the correlation function between the f and c orbitals on the same site. The negative value of the correlation function suggests the antiferromagnetic coupling between the f orbital and c orbital. As shown in Fig. 2(d), the absolute value of correlation increases in the AF2 phase as E_f increases. We have shown that the local moments of both f orbitals and c orbitals are decreasing. The increasing on the correlation magnitude indicates the formation of Kondo singlet even in the antiferromagnetic phase. It reaches maximum at the Lifshitz transition point, and in the AF1 phase it decreases. In the PKS phase, the correlation approaches zero as E_f increases. Due to the formation of Kondo singlet between the f orbitals and c orbitals, the correlation has a non-zero value. However in the $E_f \to \infty$ limit, all the electrons occupy the c orbitals, so $C_{fd}(r = 0)$ is approaching zero.

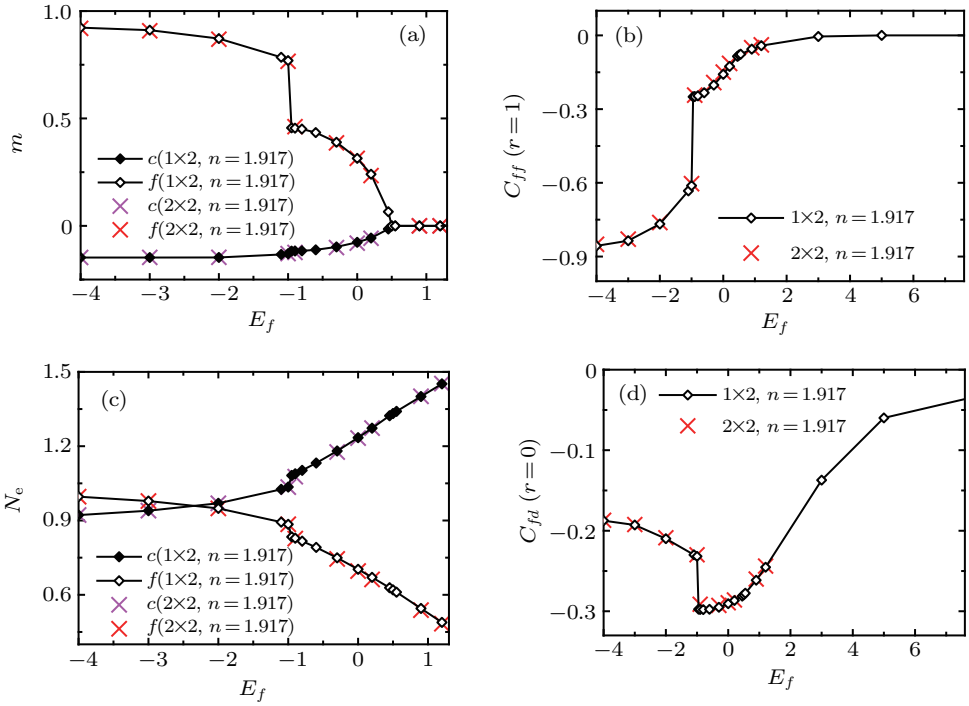


Fig. 2. (color online) Different physical quantities as a function of E_f at filling $n = 1.917$ and $V = 0.9$. Contributions of the conduction c orbitals and localized f orbitals to (a) the magnetic moment and (c) number of electrons. The black solid line with solid (hollow) circles is the contribution from the f orbital (c orbital) when the cluster size is 1×2, and the red (purple) symbols are the contribution from the f orbitals (c orbitals) when the cluster size is 2×2. (b) Correlation function between two neighboring f orbitals, $C_{ff}(r = 1)$. (d) The on-site f and c orbitals correlation, $C_{fd}(r = 0)$. Cluster size 1×2 results are labeled by the black solid line with hollow circles, and the 2×2 results are labeled by the red symbols.

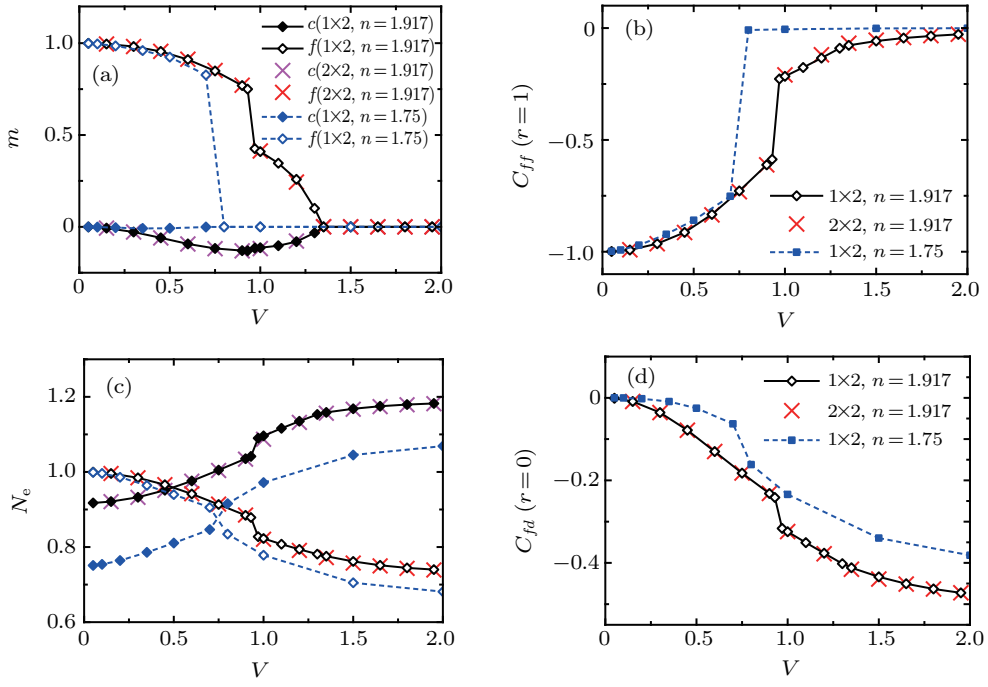


Fig. 3. (color online) Physical quantities as a function of V when $E_f = -1$ at different fillings. Contributions of the conduction c orbitals and localized f orbitals to (a) the magnetic moment and (c) the number of electrons. The labels are the same as those in Fig. (a), except that the blue dashed line with solid (hollow) circles is the contributions from the f orbital (c orbital) at filling $n = 1.75$ when the cluster size is 1×2. (b) The correlation function between two neighboring f orbitals, $C_{ff}(r = 1)$. (d) The on-site f and c orbital correlation, $C_{fd}(r = 0)$. The blue dashed line with solid circles is the results from filling $n = 1.75$ when the cluster size is 1×2. The rest of the labels are the same as those in Fig. 2(b).

It is interesting to examine $C_{fd}(r = 0)$ in the AF1 phase. We mentioned that the Kondo singlet state is formed even in the AF2 phase, this should occur in the AF1 phase too. The correlation function decreases slowly in this phase. The reason is that the contribution from antiferromagnetic becomes weak, and at the same time the number of f electrons de-

creases rapidly, the number of Kondo singlet pairs also decreases. In the PKS phase, the number of f electrons decreases further, so the correlation function decreases fast.

Next we fix the on-site energy of the f orbital $E_f = -1$ at filling $n = 1.75$ and $n = 1.917$ (along the vertical dashed line in Figs. 1(a) and 1(b)), the results are displayed in Fig. 3. Since the Kondo coupling $J_K \propto V^2$, at small (large) V, the Kondo coupling is weak (strong). When the Kondo coupling is weak, the RKKY coupling dominates, and the antiferromagnetic long range order appears. As V increases, the Kondo coupling dominates, and the AF order is destroyed. Now we discuss the results at different fillings in detail.

At filling $n = 1.917$, the competition of RKKY coupling and Kondo coupling leads to the AF1 phase. At small V, the RKKY coupling dominates, and the AF2 order is formed. As V increases to the intermediate region, the AF1 phase appears, and at large V, the Kondo singlet is formed between the f orbitals and c orbitals. The local moment is shown in Fig. 3(a), the m_f–V curve is quite similar to the m_f–E_f curve. However the local moment of the c orbitals, m_c, is slightly different. In the AF2 phase, it increases as V increases, and reaches maximum at the Lifshitz transition point. The behavior of the correlation between two neighboring f orbitals is also similar to that in the $C_{ff}(r = 1)$–E_f curve. The number of electrons is also varying as V changes, since the effect of V is to mix the two orbitals, and the on-site U makes the electrons be more likely to occupy the c orbitals. In the PKS phase, the numbers of electrons in different orbitals only change a little bit. The correlation between the f and c orbitals on the same site keep increasing as V increases. As $V \to \infty$, it approaches -0.5.

While at filling $n = 1.75$, when $E_f = -1$ the AF1 phase does not exist. The transition between the AF2 phase and PKS phase is of first order, since the forms of Fermi surface are different in the two phases. There is a big step in both the f orbital local moment curve and the $C_{ff}(r = 1)$ curve. The local moment of the c orbital is close to zero in the AF2 phase. The local magnetic moment of the f orbital and the correlation of the f orbitals are zero in the PKS phase. The behavior of the number of electrons is quite similar to that at filling $n = 1.917$, except that the jump is not so obvious. Since the local moment of the c orbital is almost zero in the AF2 phase, the correlation of the on-site c and f orbitals is close to zero too. The magnitude of correlation increases slightly as V increases, in the PKS phase the magnitude of correlation increases rapidly.

In the end, we discuss the Lifshitz transition. As we mentioned previously, the phase transition is caused by the Fermi surface reconstruction. By using the variational Monte Carlo method, Wanabe *et al.*[11] calculated the momentum distribution functions of different phases. They found that the f orbital does not contribute to the formation of Fermi surface in the AF2 phase. This indicates that the f orbital is completely localized in the AF2 phase. But it becomes itinerant in the AF1 phase as well the PKS phase. Other evidence of Fermi surface reconstruction is from the study of cellular dynamical mean field theory by De Leo *et al.*[34] They found that the AF2–AF1 transition is accompanied by a rearrangement of spectral weight. We find a discontinuity in both the magnetic moments and the number of electrons. In Fig. 4, the evolution of the magnetic moment versus E_f at different fillings is shown. At the transition point between the AF2 and AF1 phases, there are steps in both the m_f curve and the m_c curve. The latter is much smaller, which can hardly be seen in the figure. It is very clear that as it approaches half filling, the step of m_f becomes smaller and smaller. The inset of Fig. 4 shows the magnitude of the step on m_f. The step decreases as the filling increases, and becomes zero when the filling reaches half filling. At half filling, there is no difference between the AF2 and AF1 phases.

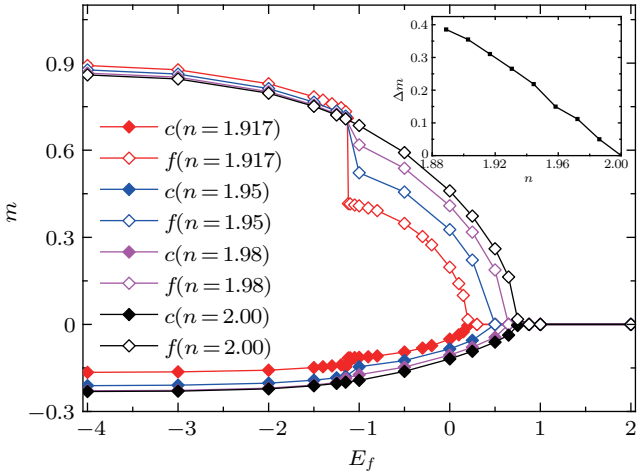


Fig. 4. (color online) Magnetic moment m as a function of E_f at different filling and $V = 1.0$. Hollow (solid) diamonds are the contributions of the f orbital (c orbital) to the magnetic moment. Red, blue, purple, and black lines are the results at filling $n = 1.917$, $n = 1.95$, $n = 1.98$, and $n = 2.0$, respectively. Both m_f and m_i have a finite step at the Lifshitz transition point, and the magnitudes of the steps of m_f at different fillings are shown in the inset. As the filling approaches half filling, the step vanishes.

The Fermi surface topology in different phases is plotted in Fig. 5. The PKS phase is the ordinary Fermi liquid state with a large Fermi surface. Since the antiferromagnetic long range order is present, the Brillouin zone is halved in the AF1 and AF2 phases. The lower band is completely full, while the upper band is partially filled. The Fermi surface of the AF1 phase has a hole pocket, and it has an electron pocket in the AF2 phase. The hole-like Fermi surface of the AF1 phase can be obtained by folding the Fermi surface in the PKS phase. Therefore the AF1 phase and the PKS phase are smoothly connected with each other, the phase transition between the two phases is of second order. The Fermi surface topology in the AF2 phase is different, thus the transitions from the AF2 phase to the other two phases are of first order. Since the model has

particle–hole symmetry at half filling, the difference between the AF1 phase and AF2 phase disappears.

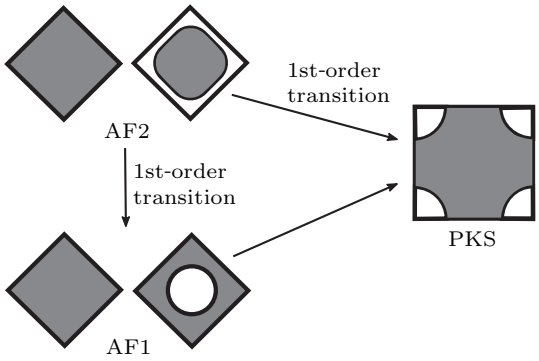


Fig. 5. Schematic plot of Fermi surface in the three different phases. In the AF2 phase, the Fermi surface has an electron pocket. The Fermi surface of the AF1 phase has a hole pocket, it can be obtained by folding the Fermi surface in the PKS phase.

4. Conclusion

In summary, we applied the density matrix embedding theory to the two-dimensional periodic Anderson model. We mainly concentrated on the ground state properties. We systematically investigated the phase transitions between the AF2 phase, AF1 phase, and PKS phase. The phase transition from the AF1 phase to PKS phase is just the ordinary magnetic transition, while the phase transitions from the AF2 phase to the other two phases are of first order, which are accompanied by a Fermi surface reconstruction. We obtained the V–E_f phase diagrams at different fillings, and found that as the filling is getting close to the half filling, the AF2 phase is shrinking while the AF1 phase is expanding. In order to characterize different phases, we computed the local magnetic moments as well as the short-range spin–spin correlation functions. There are regions where the antiferromagnetic long-range order presents, as the magnitudes of the local moments on both c and f orbitals are decreasing, while the absolute value of the spin–spin correlation function is increasing. This indicates that the AF order coexists with the Kondo singlet phase. We further compared the local magnetic moments at different fillings, and discovered that the difference of the AF2 phase and AF1 phase is disappearing as we approach the half filling. This behavior is similar to the water liquid–vapor transition. Before the critical point, the phase transition between the liquid phase and gaseous phase is of first order. The difference of the two phases is the density. However after the critical point, the densities of the two phases become the same, there is no way to distinguish them. The AF2 phase and AF1 phase are just like the liquid water phase and the gaseous water phase. The phase transition of the AF2 phase and AF1 phase is not accompanied by any symmetry breaking. There exists a quantum critical point at half filling or quite close to half filling.

References

[1] Stewart G R 1984 *Rev. Mod. Phys.* **56** 755
[2] Andres K, Graebner J E and Ott H R 1975 *Phys. Rev. Lett.* **35** 1779
[3] Thompson J D and Fisk Z 2012 *J. Phys. Soc. Jpn.* **81** 011002
[4] Van Dyke J S, Massee F, Allan M P, Davis J C S, Petrovic C and Morr D K 2014 *Proc. Nat. Acad. Sci. USA* **111** 11663
[5] Chen Y, Weng Z F, Michael S, Lu X and Yuan H Q 2016 *Chin. Phys. B* **25** 077401
[6] Shen B, Yu L, Liu K, Lyu S P, Jia X W, Bauer E D, Thompson J D, Zhang Y, Wang C L, Hu C, Ding Y, Sun X, Hu Y, Liu J, Gao Q, Zhao L, Liu G D, Xu Z Y, Chen C T, Lu Z Y and Zhou X J 2017 *Chin. Phys. B* **26** 077401
[7] Stewart G R 2001 *Rev. Mod. Phys.* **73** 797
[8] Anderson P W 1961 *Phys. Rev.* **124** 41
[9] Shinzaki R, Nasu J and Koga A 2016 *J. Phys. Soc. Jpn.* **683** 012041
[10] Kubo K 2015 *J. Phys. Soc. Jpn.* **84** 094702
[11] Watanabe H and Ogata M 2009 *J. Phys. Soc. Jpn.* **78** 024715
[12] Wysokisnski M M, Abram M and Spalek J 2014 *Phys. Rev. B* **90** 081114
[13] Vekic M, Cannon J W, Scalapino D J, Scalettar R T and Sugar R L 1995 *Phys. Rev. Lett.* **74** 2367
[14] Lin H F, Tao H S, Guo W X and Liu W M 2015 *Chin. Phys. B* **24** 057101
[15] Hu W, Scalettar R T, Huang E W and Moritz B 2017 *Phys. Rev. B* **95** 235122
[16] Lifshitz I M 1960 *Sov. Phys. JETP* **11** 1130
[17] Paschen S, Luehmann T, Wirth S, Gegenwart P, Trovarelli O, Geibel C, Steglich F, Coleman P and Si Q 2004 *Nature* **432** 881
[18] Goh S K, Paglione J, Sutherland M, O'Farrell E C T, Bergemann C, Sayles T A and Maple M B 2008 *Phys. Rev. Lett.* **101** 056402
[19] Jiao L, Chen Y, Kohama Y, Graf D, Bauer E D, Singleton J, Zhu J X, Weng Z, Pang G, Shang T, Zhang J, Lee H O, Park T, Jaime M, Thompson J D, Steglich F, Si Q and Yuan H Q 2015 *Proc. Nat. Acad. Sci. USA* **112** 673
[20] Chatterjee S, Ruf J P, Wei H I, Finkelstein K D, Schlom D G and Shen K M 2017 *Nat. Commun.* **8** 852
[21] Watanabe H and Ogata M 2007 *Phys. Rev. Lett.* **99** 136401
[22] Li H, Liu Y, Zhang G M and Yu L 2015 *J. Phys.: Condens. Matter* **27** 425601
[23] Zhang G M, Su Y H and Yu L 2011 *Phys. Rev. B* **83** 033102
[24] Knizia G and Chan G K 2012 *Phys. Rev. Lett.* **109** 186404
[25] Booth G H and Chan G K 2015 *Phys. Rev. B* **91** 155107
[26] Zheng B X and Chan G K 2016 *Phys. Rev. B* **93** 035126
[27] Zheng B X, Kretchmer J S, Shi H, Zhang S and Chan G K 2017 *Phys. Rev. B* **95** 045103
[28] Chen Q N, Booth G H, Sharma S, Knizia G and Chan G K 2014 *Phys. Rev. B* **89** 165134
[29] Sandhoefer B and Chan G K 2016 *Phys. Rev. B* **94** 085115
[30] Knizia G and Chan G K 2013 *J. Chem. Theory Comput.* **9** 1428
[31] Sun Q M and Chan G K 2014 *J. Chem. Theory Comput.* **10** 3784
[32] Wouters S, Jimnez-Hoyos C A, Sun Q M and Chan G K 2016 *J. Chem. Theory Comput.* **12** 2706
[33] Sharma S and Chan G K 2012 *J. Chem. Phys.* **136** 124121
[34] Leo L D, Civelli M and Kotliar G 2008 *Phys. Rev. B* **77** 075107